ChemSusChem

Research Article
doi.org/10.1002/cssc.202301614

Chemistry Europe
European Chemical Societies Publishing

www.chemsuschem.org

Long-Term Stability of Light-Induced Ti^{3+} Defects in TiO_2 Nanotubes for Amplified Photoelectrochemical Water Splitting

Ewa Wierzbicka,*[a] Ewelina Szaniawska-Białas,[a] Thorsten Schultz,[b, c] Amanda O. Basilio,[d] Dariusz Siemiaszko,[a] Kallol Ray,[d] Norbert Koch,[b, c] Nicola Pinna,[e] and Marek Polański[a]

This study shows that the simple approach of keeping anodic TiO_2 nanotubes at 70 °C in ethanol for 1 h results in improved photoelectrochemical water splitting activity due to initiation of crystallization in the material amplified by the light-induced formation of a Ti^{3+}–V_o states under UV 365 nm illumination. For the first time, the light-induced Ti^{3+}–V_o states are generated when oxygen is present in the reaction solution and are stable when in contact with air (oxygen) for a long time (two months). We confirmed here that the amorphous or nearly amorphous structure of titania supports the survival of Ti^{3+} species in contact with oxygen. It is also shown that the ethanol treatment substantially improves the morphology of the titania nanotube arrays, specifically, less surface cracking and surface purification from C- and F-based contamination from the electrolyte used for anodizing.

Introduction

Since the work of X. Chen, S.S. Mao, et al. in 2011,[1] the reduction of titanium dioxide (TiO_2) has received increasing attention as a novel approach to the so-called self-doping of titania with Ti^{3+}–V_o point defects that causes coloration and serve as the active catalytic centers.[2–4] Some further investigations show that the material coloration and, therefore, visible light absorption does not contribute to the photocatalytic (PC) and photoelectrochemical (PEC) hydrogen evolution processes. That is, although visible light is absorbed, these excited electrons recombine to the ground state, and no visible light-driven reaction takes place.[3,5] The improved PC activity of the surface-reduced material is due to an extra electronic state of Ti^{3+} located slightly below the conduction band of titania, which traps electrons and mediates their transfer at the interface with an electrolyte.[6] On the other hand, PEC processes benefit from the improved conductivity[5,7,8] and much higher carrier density that result from the presence of Ti^{3+} states.[9]

Another aspect of the reductive treatment is forming an amorphous shell or disordered surface layer, which was initially identified as the cause of the improved PC/PEC activity.[1,10,11] However, the surface amorphization become a matter of debate. For example, titania commercial powders with a rather rough surface exhibit surface amorphization, while single crystals[3,12] and hydrothermal powders with well-defined facets do not exhibit, but only point defect formation.[13] Additionally, it was confirmed that different titania polymorphs show varied behaviors towards reductive treatments, i.e., brookite is more readily reduced compared to anatase and rutile.[3] This is attributed to the fact that brookite has the most disordered crystalline structure of the three polymorphs. Therefore, a certain trend may be discerned from previous works; the higher the titania structural disorder, the easier Ti^{3+} species are formed.

Recently, an important synthesis strategy employs the Ti^{3+} centers as trapping surface defects for single-atom (SA) noble metal deposition. A considerable number of publications have shown that a minimal loading of precious metals onto titania can result in outstanding PEC/PC performances.[14–16] Therefore, straightforward synthesis methods of Ti^{3+} states in titania are still intensively searched for. Among the approaches to reduced titania, the vast majority of previous studies apply reductive

[a] Dr. E. Wierzbicka, Dr. E. Szaniawska-Białas, Dr. D. Siemiaszko, Prof. Dr. M. Polański
Department of Functional Materials and Hydrogen Technology, Faculty of Advanced Technologies and Chemistry
Military University of Technology
Kaliskiego Street 2, 00908 Warsaw, Poland
E-mail: ewa.wierzbicka@wat.edu.pl

[b] Dr. T. Schultz, Prof. Dr. N. Koch
Institut für Physik and IRIS Adlershof
Humboldt-Universität zu Berlin
Brook-Taylor-Str. 6, 12489 Berlin, Germany

[c] Dr. T. Schultz, Prof. Dr. N. Koch
Helmholtz-Zentrum Berlin für Materialien und Energie GmbH
Hahn-Meitner-Platz 1, 14109 Berlin, Germany

[d] A. O. Basilio, Prof. Dr. K. Ray
Institut für Chemie,
Humboldt-Universität zu Berlin
Brook-Taylor-Str. 2, 12489 Berlin, Germany

[e] Prof. Dr. N. Pinna
Department of Chemistry, IRIS Adlershof & The Center for the Science of Materials Berlin
Humboldt-Universität zu Berlin
Brook-Taylor-Str. 2, 12489 Berlin, Germany

Supporting information for this article is available on the WWW under https://doi.org/10.1002/cssc.202301614

Research Article
doi.org/10.1002/cssc.202301614

annealing in a H_2 or H_2/Ar at elevated temperatures (300–1000 °C).[2,17,18] However, introducing oxygen vacancies (Vo) and forming Ti^{3+} centers in the TiO_2 lattice can also be achieved by other methods, such as wet chemistry, ultrasonication, and gel combustion.[19] A facile way to form Ti^{3+} centers is the simple light illumination of crystalline anatase in an oxygen-free solution (water-methanol mixture).[5,20] Indeed, it was confirmed that although the PC hydrogen evolution exponentially increased due to the constant rise in the concentration of Ti^{3+} under light exposure, the defect disappeared immediately upon air exposure (the sample also reverted to white color). Thus, despite the simplicity of this method, the lack of stability of the Ti^{3+} centers is the main obstacle hindering the application of this type of reductive treatment.

This work introduces a mild pre-annealing treatment that reduces surface cracking and material contaminations. For this purpose, the as-anodized TiO_2 nanotube arrays were kept in ethanol at 70 °C from 1 to 24 h. On top of clear improvements in morphology and purity, the treatment resulted in improved PEC water-splitting activity related to Ti^{3+} defect formation under UV light illumination and low-temperature initiation of the crystallization of the material. In contrast to previous studies,[5,20] the light-induced Ti^{3+} cocatalytic centers remained stable after long-term oxygen exposure (2 months). Electron paramagnetic resonance (EPR) spectroscopy studies confirmed that this phenomenon was related to titania's amorphous/almost amorphous structure that stabilizes the surface Ti^{3+} centers. As an important outlook alternative to the high-temperature hydrogen annealing typically used to create Ti^{3+} centers, our straightforward procedure can be utilized for single-atom cocatalyst deposition, which is currently attracting considerable attention from the PC/PEC community.

Results and Discussion

The primary purpose of this work was to identify a mild pre-annealing treatment to apply before annealing in air (450 °C 1 h, to induce crystallization to the TiO_2 anatase polymorph) to eliminate surface cracking and organic contamination from the TiO_2 nanotube surface. First, we tried to apply a previously reported treatment known as water annealing,[21] in our case at 70 °C for 1 h, followed by a standard annealing in air. However, this approach resulted in the titania nanotube layer entirely peeling off from the Ti metal (see Figure S1, WA). Therefore, we decided to replace water with ethanol as the solvent to remove the ethylene glycol and NH_4F electrolyte from the titania nanopores. In this approach, after washing in cold EtOH three times, the samples were directly transferred to EtOH at 70 °C under stirring (no drying in between) for 1 h. This additional EtOH treatment resulted in less surface contamination than observed for the as-anodized samples after annealing under the same conditions (Figure S1, AA, and EA samples). The EtOH-treated and annealed sample (EA) showed a uniform violet color, while the as-anodized and annealed (AA) top was covered with a green organic byproduct residual layer (see the XPS results in the following section). In contrast to the samples obtained after treatment in water, the surface of the tubes remained well adhered to the substrate. Additionally, SEM analysis of the specimens from the top view shows that the number of surface cracks was reduced for both types of samples before and after annealing in air when the treatment in EtOH was applied (Figure 1). The effect was most apparent in the low-magnification images (Figure 1m, n). Besides these observations, the samples showed similar morphologies with nanopore diameters of 70–100 nm and thicknesses of ~12 μM (Figure S2).

Figure 2a shows an overview of the photoelectrochemical water splitting performance of amorphous TiO_2 nanotubes in 0.1 M Na_2SO_4 under chopped UV light (365 nm) illumination and at a positive 0.6 V bias vs. Ag/AgCl (1.25 V vs. RHE).

For samples subjected to EtOH for up to 24 h (E(1 h), E(6 h), E(24 h)), clear photocurrent responses were observed, as well as strong photocurrent amplification in the initial on-off illumination cycles. At the same time, the as-anodized samples show only residual (baseline) photocurrent response (A_1st and A_2nd, the orange plots). This confirms that the EtOH treatment is the key step for the PEC activation of samples.

The activation of the EtOH-treated samples after different immersion times was very similar. After the first light impulse, the photocurrent density reached the same values. However, subsequent photocurrent transients showed slightly higher improvement for the nanotubes that underwent longer EtOH treatment. In all cases, after every 5–6 on/off cycles, the photocurrent density reached maximum values and stabilized. A positive influence was observed for both light current increasing and dark current decreasing. The effect was reproducible and rather stable over 40 on/off illumination cycles (Figure 2b). Interestingly, after removing the sample from the solution, a black spot appeared on the sample surface that was exposed to UV light illumination (Figure 2c). This was found to be caused by light-induced defects Ti^{3+}–V_o (later confirmed by EPR studies). Such defects were, for the first time, formed in the presence of oxygen (no sacrificial agent was used, nor was oxygen removed from the solution). In addition, the defects have been remarkably resistant to prolonged exposure to air in contrast to previously reported light-induced Ti^{3+} states.[5,20] Another important fact is that the as-anodized samples (A) also acquired a stable black color without photocatalytic activation, as shown in Figure 2a. This strongly suggests that low-temperature EtOH treatment at 70 °C, for as little as 1 h, has a beneficial influence on the material, working synergistically with light activation (stable Ti^{3+}–V_o state formation) to amplify the PEC water splitting performance. Although the sample color became dark black, the morphological features remained unchanged after illumination (see Figure 1e–h).

Next, XRD measurements were conducted to preliminarily assess the amorphous/crystalline nature of the bulk materials on two series of samples, as-anodized (A) and 1 h EtOH-treated E(1 h), before and after 2 h of continuous illumination (365 nm LED, 30 mWcm^{-2}) in distilled water (samples AI and EI, respectively) and after 1 h of air annealing at 450 °C followed by 2 h of continuous illumination (AAI and EAI, respectively). Consistent with the expectations, the results showed the

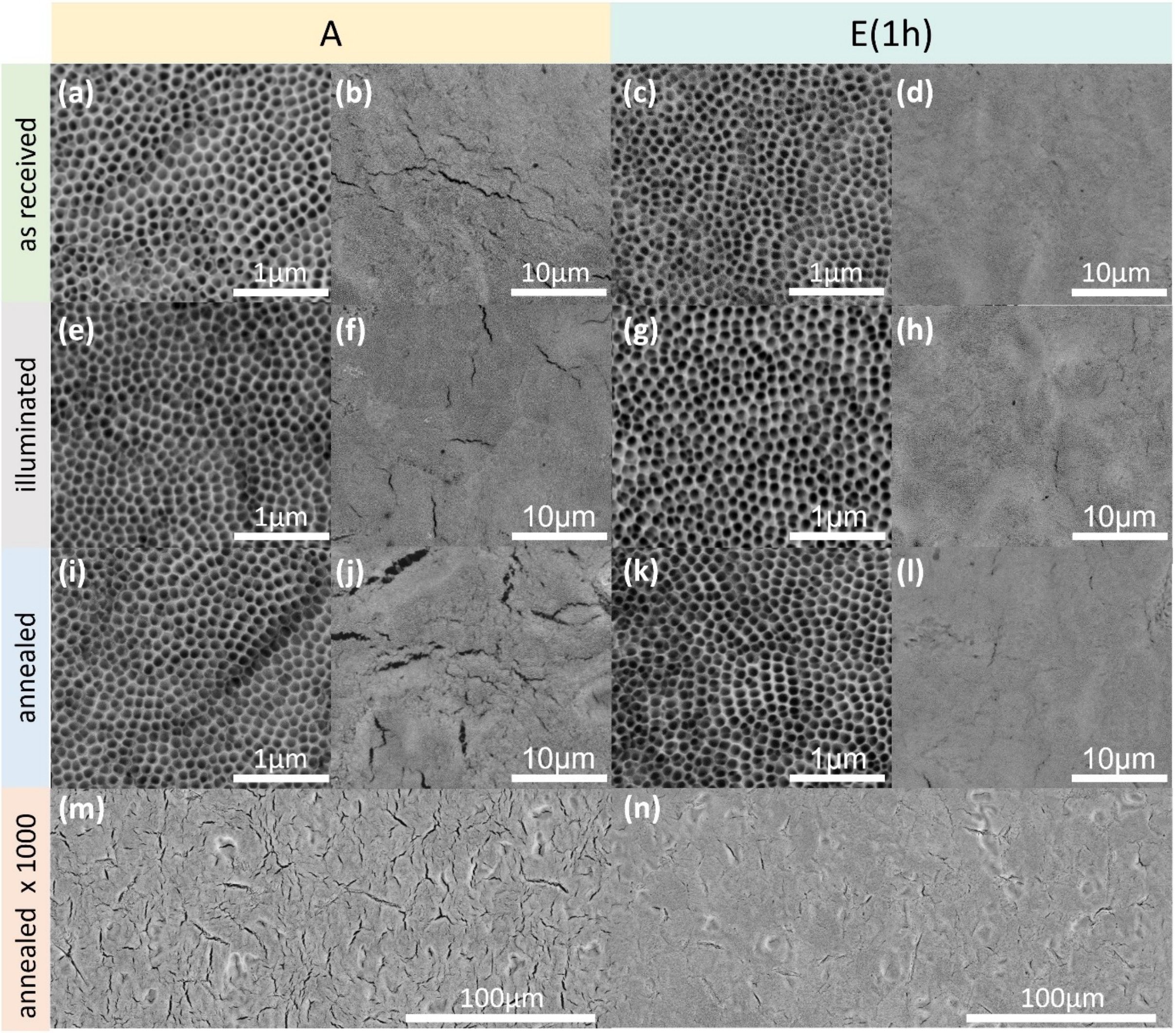

Figure 1. SEM images of anodic TiO_2 nanotube arrays: series A represent as-anodized samples, series E(1 h) represent samples after an additional 1 h treatment in EtOH at 70 °C. The sample morphology was evaluated (a–d) immediately after the samples were obtained or after additional posttreatment steps: (e–h) UV (365 nm) LED illumination, (i–l) 1 h annealing in air at 450 °C, and (m–n) annealed samples at low magnification to see the top view of the titania nanotube morphology.

amorphous character of the as-anodized and EtOH-treated samples before and after illumination (A, AI, E(1 h), EI) and the anatase phase of the air-annealed samples (AAI, EAI); see Figure S3.

The same series of samples were also analyzed by EPR, enabling the detection of Ti^{3+} species. It is very important to emphasize that for these measurements, all samples were prepared by illumination of the TiO_2 nanotube immersed in water (containing oxygen), and moreover, between the samples preparation and the EPR measurements, they were stored in air (exposed to oxygen) for two months. This allowed us to obtain information on both the Ti^{3+} defect formation and their long-term stability in contact with oxygen. The EPR spectra of all measured samples are presented in Figure 2 d-i and S4. The reference samples without illumination (A and E(1 h), Figure 2d and g respectively), showed only poorly defined and relatively low intense EPR signals around a *g*-value of 2, which is characteristic of naturally present paramagnetic Ti^{3+} ($3d^1$, $S=\frac{1}{2}$) sites in titania. On the other hand, the spectra of both amorphous samples after illumination - black TiO_2 nanotube (AI, Figure 2e and EI, Figure 2h) showed well-defined EPR isotropic signals centered at a *g*-value of 1.94, typically assigned to Ti^{3+} surface states, formed by reductive treatment.[2,22] This clearly confirms that in the amorphous state, the Ti^{3+} sites are formed even in the presence of oxygen and survive long-term air exposure (at least 2 months). It was confirmed before that such light-induced Ti^{3+} states in anatase activate PC H_2 evolution and improve PEC water splitting, but particularly interesting is the fact that they were unstable in contact with oxygen (being stable only in an oxygen-free solution and disappearing immediately after air exposure).[5] To prove that this is also the case for crystalline titania nanotubes used in our studies, anatase samples (annealed in air at 450 °C for 1 h) and samples illuminated for 2 h (AAI, EAI) were tested for paramagnetic

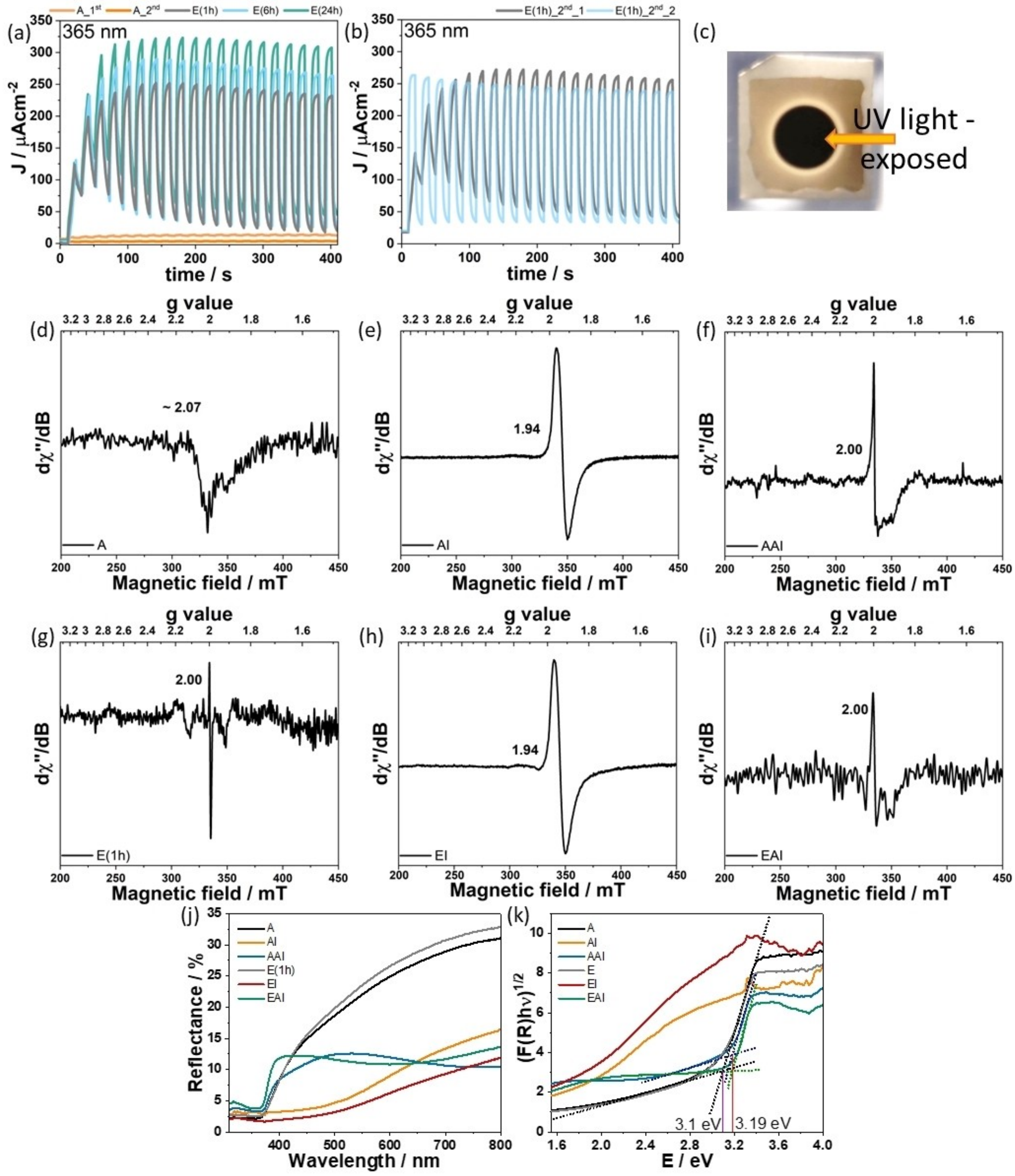

Figure 2. (a) Transient photocurrent responses of the titania nanotube photoanode obtained under different conditions: A- as-anodized samples (1st and 2nd), E(1 h), E(6 h), E(24 h) – treated in EtOH at 70 °C for 1 h, 6 h, and 24 h, respectively. (b) Reproducibility and stability tests were conducted for the second E(1 h) sample. Photocurrents were measured under 365 nm LED illumination and constant potentials of 0.6 V vs. Ag/AgCl in a 0.1 M Na_2SO_4 solution. (c) Macrophotography of the titania nanotube E(1 h) sample after PEC tests with a black spot formed after UV light exposure. EPR measurements of the samples prepared under different conditions: (d) A- as-anodized, (e) AI- as anodized and 2 h UV illuminated in DI water, (f) AAI- as anodized, annealed 450 °C for 1 h in air and 2 h UV illuminated in DI water, and analogous series for ethanol-treated samples (g) E(1 h), (h) EI, (i) EAI. EPR measurements were conducted after 2 months of sample storage in air. (j) Reflectance spectra of the samples, and (k) band gap evaluation from spectra in (j).

resonance. As expected, the light-induced defects in the material after crystallization were not detected by EPR (Figure 2f and i)). This observation proves that an amorphous structure (or nearly amorphous, as discussed in the following section of TEM results) is the only suitable environment to prevent light-induced Ti^{3+} state reoxidation, even after a long-time oxygen exposure. In light of these results and previous findings, which show that in brookite, the most disordered polymorph of TiO_2, Ti^{3+} formation happened much faster than in other polymorphs,[3] we can confirm that with greater disorder of the structure, the formation and stability of the Ti^{3+} centers are more facilitated. The formation of Ti^{3+} centers that lead to the color change[23] was studied by DRS measurements (Figure 2j, k). In line with the EPR results, only the AI and EI samples showed increased absorption over the entire visible light range, while the illuminated crystalline titania nanotubes did not exhibit any shift in optical absorption.[24] The band-gap values determined for the reference samples with and without EtOH

Research Article
doi.org/10.1002/cssc.202301614

treatment (A and E(1 h)) showed the same value of 3.1 eV. Due to the presence of Ti^{3+} surface states in the colored samples, band-gap determination using the Kubelka-Munk function would not be suitable.[25]

Additionally, in situ electrochemical impedance spectroscopy measurements were conducted to explore the charge carrier kinetics, both in the dark and after different intervals of UV light irradiation. After measuring the samples in the dark, the UV light was turned on for defined time intervals but switched off before the EIS measurements (dark measurement conditions) to determine the light-induced permanent changes in the sample without any photoelectrochemical reactions taking place during the measurement. To interpret the Nyquist and Bode plots, equivalent circuit model systems were selected for spectral fittings (insets in Figure 3a, d). The corresponding electrochemical parameters of the elements used to fit the experimental data are presented in Table S1.

As shown in Figure 3, a very different behavior was observed for the in situ illuminated as-anodized and 1 h EtOH-treated samples (A and E(1 h)). Basically, the impedance spectra of the as-anodized samples showed very little difference after illumination. From the Bode plots, it can be seen that the total impedance modulus remained almost constant at high impedance values for low frequencies ($|Z|_{10mHz}$ is between 0.6 and $0.8 \cdot 10^5\ \Omega$). Analogously, the phase shift diagrams also showed only a minimal influence of light illumination, indicating that the formation of Ti^{3+} (although confirmed by EPR) in these samples had almost no effect on the charge transfer properties. There are two time constants in the low- and high-frequency ranges, which can be attributed to the electrochemical double layer and space charge layer at the semiconductor/Ti metal interface, respectively.[26,27] Therefore, the equivalent circuit model includes the following elements: R_{CT} assigned to the charge transfer resistance parallel to a constant phase element (CPE), describing the double layer capacitance (Q_{dl}), and Q_{SC} and R_{SC} representing the space charge capacitance and resistance in the high-frequency range, respectively. Moreover, all the presented models included R_s elements corresponding to electrolyte resistance.

Significantly different behavior was observed when low-temperature EtOH treatment was applied to the titania samples. After 10 minutes of UV illumination, the resistance decreased by two orders of magnitude, from $|Z|_{10mHz} = 5.03 \cdot 10^4\ \Omega$ to $|Z|_{10mHz} = 8.03 \cdot 10^2\ \Omega$, and continued to slightly decrease for the next 4 h of illumination. A smaller semicircle at higher frequencies in the Nyquist plot (Figure 3e) indicated much higher conductivity for the 1 h EtOH-treated samples than for the as-anodized samples (Figure 3b).[28] Here, both the space charge and charge transfer resistance values decreased with UV irradiation time, which is opposite to the results for the as-anodized samples, the values of which increased overall after some slight fluctuations. This is in line with the photoelectrochemical results, in which the EtOH-treated sample (E(1 h)) exhibited light amplification and a much higher photocurrent density than the as-anodized (A) sample (Figure 2a,b). This observation evidences that the strong resistivity drop is attributed to the change taking place in the material during low-temperature EtOH treatment. This step is the prerequisite

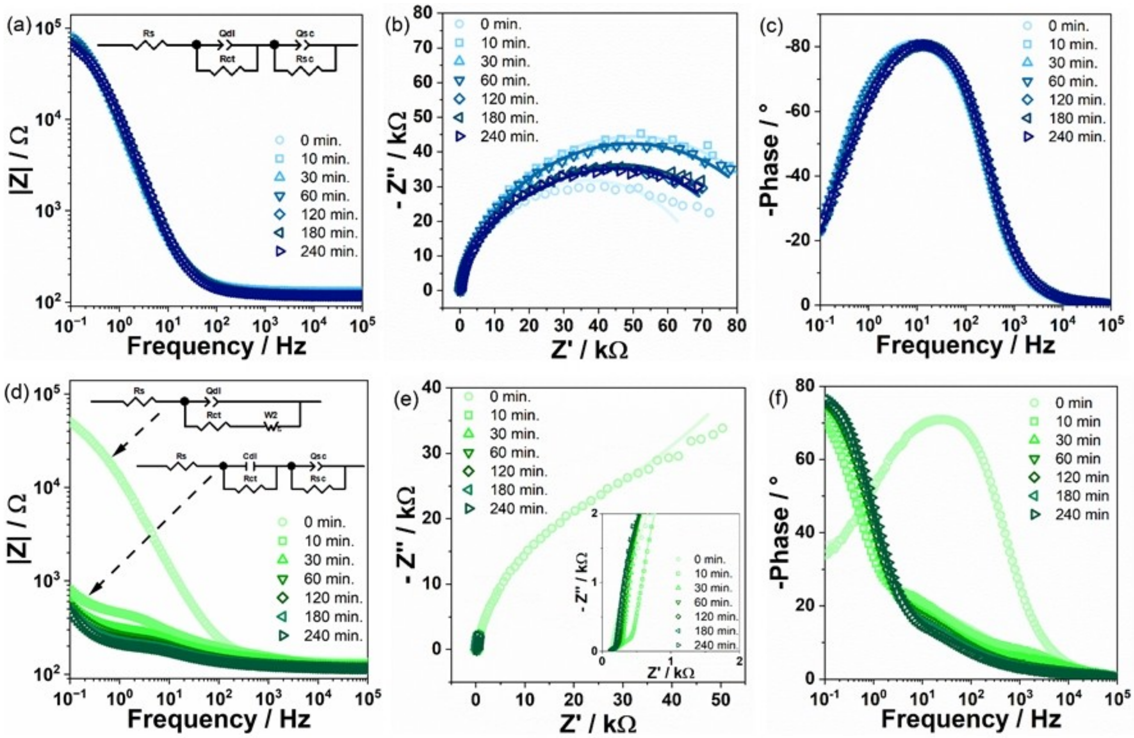

Figure 3. (a and d) Nyquist and (b, c and e, f) Bode plots fitted with simulated equivalent circuits determined for as-anodized (A), and EtOH 1 h treated samples (E(1 h)), respectively. Empty symbols correspond to the experimental data; solid lines correspond to the fitting obtained with equivalent circuits presented in (a and d).

conditioning of material for PEC activation that happened after light-induced Ti^{3+} states incorporation, that leads to a total impedance drop, and in consequence enhancing the overall PEC water-splitting activity. Based on the shape investigation of Nyquist and Bode plots, the equivalent circuit model for the E(1 h) samples based on the Randles cell (RC) was a combination of solution resistance (R_s), capacitance (Q_{dl}), and resistance (R_{CT}) related to the double layer (semiconductor/electrolyte interface).[12,29–31] Furthermore, for the (E(1 h)) sample not exposed to UV irradiation, the Warburg impedance component (W_2) was identified based on a linear increase in impedance values in the low-frequency range with a constant phase of 45°.[32] The W_2 element described the mass transport impedance and was assigned to the diffusion of charged species from the bulk of the electrolyte to the interface and through the interface layer (TNTs).

As shown from the EPR results, both the EI and AI samples showed stable in air light-induced Ti^{3+} states, but the defects had very different influences on the electrochemical (EIS results) behavior. The results mentioned above strongly indicated that only the combination of EtOH treatment and illumination enhanced titania's PEC water-splitting activity. Nevertheless, the reason for this unusual light-amplified activity of EtOH-treated samples is not yet fully explained. To identify additional factors causing the difference in the overall activation of PEC water splitting between EtOH-treated and just as-anodized samples, the titania nanotube structure was investigated by HRTEM and SAED analyses after EtOH treatment for different times (0-24 h) at 70 °C. The following set of samples was tested to verify the influence of EtOH treatment and illumination on sample crystallinity: as-anodized (A), treated with EtOH for 1 h before (E(1 h)) and after (EI) illumination, and treated with EtOH for 24 h (E(24 h)). Based on the HRTEM image of the nanotubes (Figure 4 and Figs. S5 and S6), small signs of beginning of crystallization after low-temperature EtOH treatment were observed for both samples before illumination (E(1 h)) and after illumination (EI). However, the analysis of the sample treated for 24 h strongly indicated that the EtOH treatment promotes crystallization. Here, well-defined *d*-spacings of 0.35 nm were identified as anatase (011) planes.[33] For the 1 h EtOH-treated samples, some lattice fringes were assigned to anatase (002) with a *d* spacing of 0.19 nm, while others, poorly defined and marked with dashed lines, showed rather transitional *d*-spacing values since only anatase was identified in the 24 h EtOH-treated sample (E(24 h)).

SAED analysis shows no diffraction patterns from the as-anodized and 1 h EtOH-treated samples due to the lack or very small content of the crystal phase. The only clear Debye-Scherrer rings in the SAED patterns were observed for the 24 h EtOH-treated sample. This material showed a polycrystalline character (Figure 3d inset), typical for titania nanotubes. The main Debye-Scherrer rings for TiO_2 in the samples correspond to the (011), (004), (020), (015), (024), (116), (125), (224), and (035) planes in anatase (tetragonal crystal system ICDD: 96–900-9087).[27] Based on this result, it was concluded that the structure's preliminary organization process, even before complete crystallization, was the reason for light-induced PEC activity, even for mild treatment conditions such as 1 h immersion in EtOH at 70 °C.

Photoelectron spectroscopy was used to quantify the influence of the EtOH treatment combined with light-induced Ti^{3+}–V_o defects formation. As expected, the survey spectra of the samples (Figure S7) confirmed that Ti and O were the dominant elements. For all the samples except those subjected to high-temperature annealing (450 °C, 1 h, air) and 2 h UV illumination (AAI, EAI), quite intense signals from F, N, and C were detected that originated from the electrolyte residuals (ethylene glycol and NH_4F). These XPS survey measurements also confirmed that no other species were present in the samples that could give rise to the EPR signal located at a g-value of 1.94 identified as surface-exposed Ti^{3+}. High-resolution XPS measurements were used to identify different sample species based on spectral deconvolution (Figures 5a–e, S8), as quantified in Figure 5f. Although the effects were not very pronounced, it can be seen that EtOH treatment (E(1 h), EI, EAI samples) caused surface purification and overall less C- and F-based contamination (Figure 5a, e, f). The carbon peak was deconvoluted into peaks with maxima located at ~285 eV from C–C bonds, a peak at ~286.5 eV from C–O or C–N bonds, and a peak at ~289.2 eV that corresponds to the O–C=O bonds (Figure 5e).[34,35] High-temperature air annealing (AAI and EAI samples) most efficiently helped to eliminate fluorides physically adsorbed on the surface of TiO_2 nanotubes; the single fluorine peak intensity at 684.6-684.8 eV strongly decreased after treatment (Figure 5a). In addition, the F^- doping of TiO_2 TNTs might be excluded due to the absence of a peak at approximately 688 eV.[36] Additionally, one nitrogen peak at ~402.3 eV disappeared after air annealing (the second at ~400.5 eV remains); see Figure 5d. Based on the binding energy, the nitrogen signals were assigned to N–F species, while the peak located at a lower binding energy indicated the presence of interstitial nitrogen atoms in a Ti–O–N environment.[37,38] The existence of substitutional nitrogen was excluded due to the absence of peaks at 396–398 eV.[39]

Importantly, there was no influence of illumination (titania reduction) on the elemental composition of the samples that could be detected in HR-XPS, as only one pair of doublets at approximately 459.0-459.3 and 464.7-465.0 eV (split 5.7 eV)[40,41] was found in the titanium HR spectrum, corresponding to Ti^{4+} in TiO_2 (Figure 5c). This was complimentary to the oxygen spectrum that is composed of one dominant O–Ti peak at 530.3-530.6 eV from TiO_2,[17] two carbon byproduct-related signals at ~532 eV from the O=C bond, and a small C–O peak at ~533 eV (Figure 5b).[42] The lack of signals that confirm titania reduction is in line with previous results, where the light-induced Ti^{3+} concentration was below the detection limit of XPS (therefore, detectable only by EPR measurements).[5]

Conclusions

This work offers essential insights into the advantageous outcomes stemming from the low-temperature treatment of TiO_2 nanotubes in ethanol. It was found that the very simple

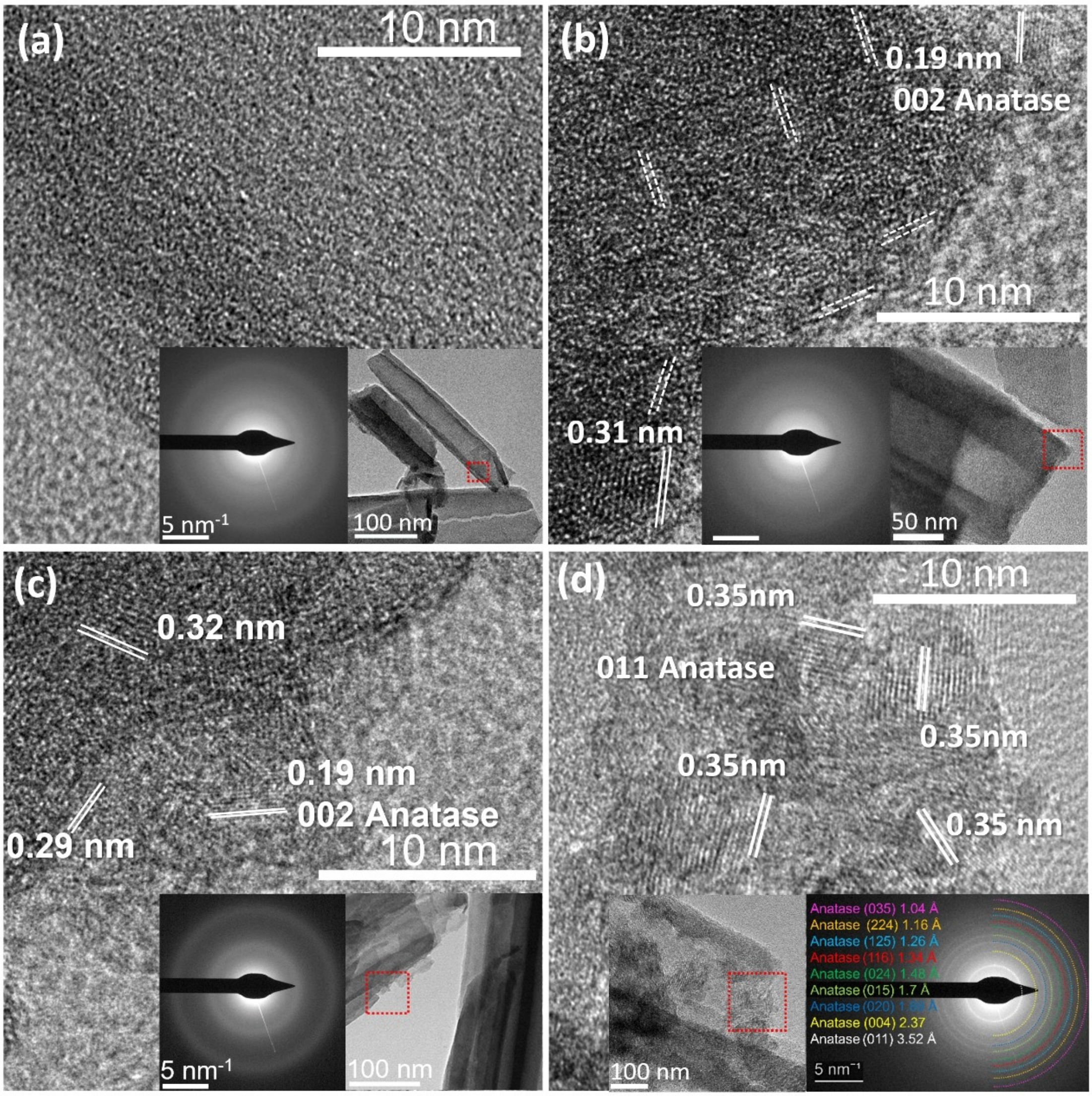

Figure 4. HRTEM micrographs of (a) A- as anodized, (b) E(1 h)- 1 h ethanol treated at 70 °C, (c) EI- 1 h ethanol treated at 70 °C and 2 h UV illuminated in DI water, (d) E(24 h)- 24 h ethanol treated at 70 °C. The images in the insets represent SAED patterns acquired from the samples.

approach of treating anodic titania nanotubes for 1 h at 70 °C in EtOH caused a clear amplified activity for photoelectrochemical water splitting. It was shown the role of the EtOH treatment is to promote slow crystallization of the titania nanotube, and following UV illumination generates Ti^{3+} cocatalytic centers (material coloration) that significantly reduce the photoanode's charge transfer resistance. These effects result in PEC activity, which is lacking in as-anodized titania. Those light-induced Ti^{3+}–V_o states were obtained in a reaction solution with oxygen and were stable when exposed to air for a long time (at least two months). This effect has been assigned to the amorphous or close to the amorphous structure of titania that supports the stabilization of Ti^{3+}–V_o centers in contact with oxygen.[6,7,11] Additionally, the primary objectives of this pre-treatment have been achieved, which is a strong improvement in titania nanotube array morphology, i.e., less surface cracking and the elimination of electrolyte residuals from the material.

Experimental

Materials synthesis

TiO_2 nanotube layers were fabricated by self-organized anodization of a Ti foil (Advent, 0.125 mm thickness, 99.6 +% purity). Before anodization, the Ti substrates were degreased by 15 min of sequential sonication in acetone, ethanol, and deionized water, followed by drying in a warm air stream. The idle area of the sample was insulated with peelable paint. A three-step anodization procedure was carried out to improve the nanopores of the anodic oxide layers. All anodization steps were carried out in an agitated (750 rpm) ethylene glycol-based (≥ 99.7%, VWR) electrolyte with 3% vol. deionized (DI) water and 0.15 M NH_4F (≥ 98%, VWR). The process was conducted using a DC power supply (Voltcraft PPS-11815) set to 60 V in a two-electrode cell with a platinum counter electrode. The oxide layers formed in the first 1 h and second 30 min anodization steps were removed from the Ti substrate by 5 min of immersion in water, a short drying process, and peeling off with adhesive tape. After the third anodization step, the samples

Research Article
doi.org/10.1002/cssc.202301614

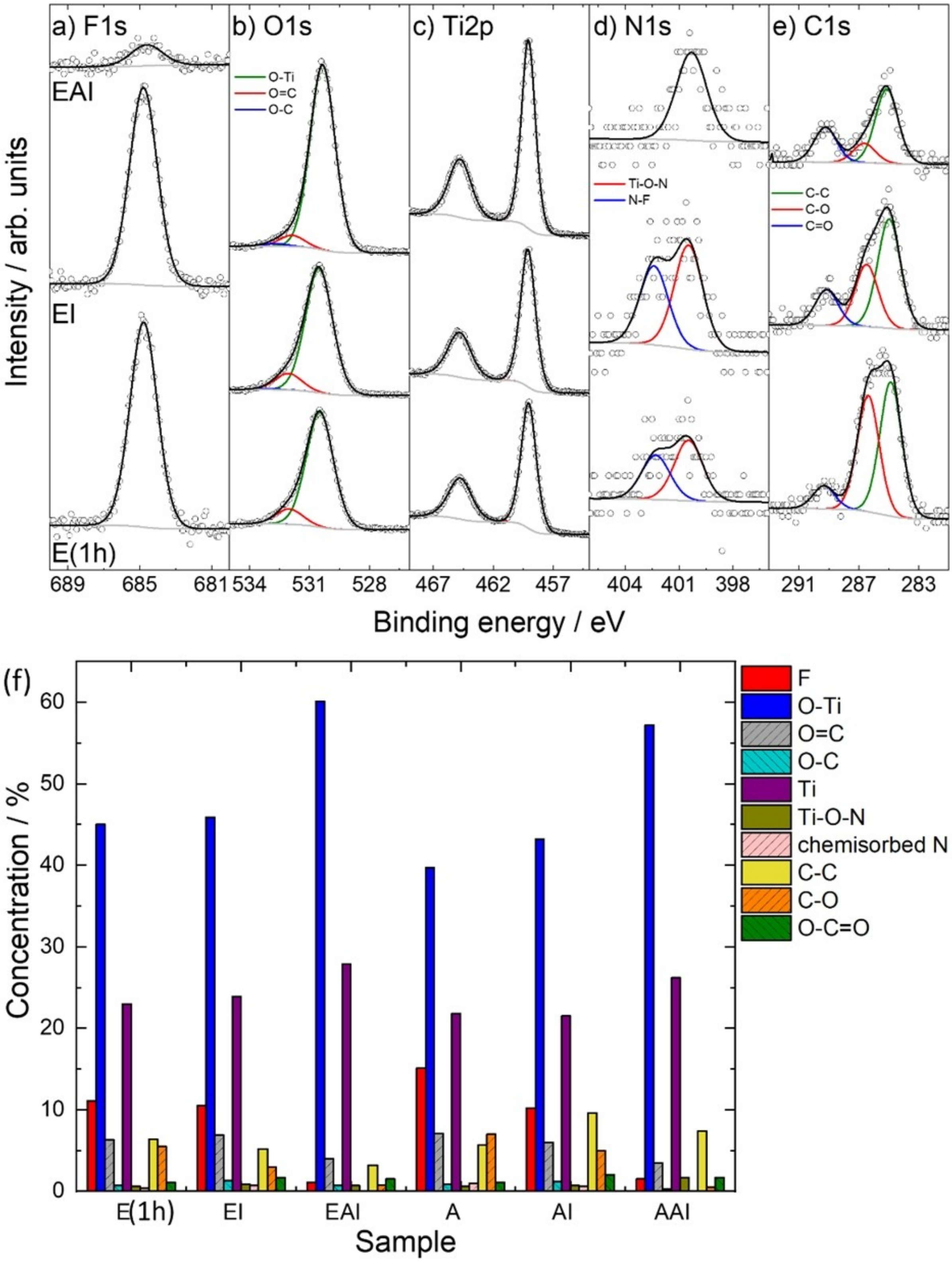

Figure 5. XPS narrow scans of a) F1s, b) O1s, c) Ti2p, d) N1s and e) C1s spectra for the E-series of samples. (b) Elemental sample composition calculated based on Figure 5a–e and S8 spectra.

were washed with ethanol; then, the "A" samples series were dried in a warm air stream, and the "E" samples series were immersed for 1–24 h in warm 70 °C ethanol with magnetic stirring (250 rpm) on a hot plate equipped with a thermocouple and then dried in warm air.

Some samples (AA and EA) were annealed in air at 450 °C for 1 h in a muffle furnace to convert the amorphous nanotubes to anatase phase. Both amorphous and crystalline samples immersed in 2 ml of deionized water (DI) water were illuminated with a UV (365 nm) LED lamp (30 $mWcm^{-2}$, ThorLabs) for 2 h.

Material Characterization

Scanning electron microscopy (SEM) (FEI, QUANTA 3D) in SE mode was used to examine the morphological features of the samples.

The photoelectrochemical performance was tested in a Teflon cell with a quartz window in a three-electrode system, where titania nanotubes on a Ti substrate were used as the working electrode (WE), a platinum wire was used as the counter electrode (CE), and an Ag/AgCl/KCl (3 M KCl) electrode was used as the reference electrode (RE). The measurements were carried out in a 0.1 M Na_2SO_4 electrolyte. Photocurrent transients were recorded under chopped light illumination (light ON/OFF 10/10 s) with a 365 nm (47 $mWcm^{-2}$) LED source (ThorLabs) and recorded with a Bio-LogicVMP3 potentiostat/galvanostat. The power of the LED was defined by means of a power and energy meter (PM100D, ThorLabs).

X-ray powder diffraction (XRD) patterns were obtained using a Rigaku ULTIMA IV diffractometer equipped with a CoK_α ($\lambda = 1.78897$ Å) radiation source operated at 40 mA and 40 kV. The data were collected in continuous mode over a 2θ range of 25–105°, with a step size of 0.5° and an acquisition rate of 1° per minute. The acquired data were processed using Origin and Match software, and the crystallographic phases were identified using the COD crystallographic database.

The continuous-wave (CW) X-band EPR spectra used for qualitative analysis of the samples were collected by means of a Bruker EMXplus instrument at a frequency of approximately 9.35 GHz in perpendicular mode. All samples for qualitative analysis were measured at an average temperature of 13 K as solid samples by using a liquid helium recirculating cooling system provided by ColdEdge.

Diffuse reflectance spectroscopy (DRS) of solid samples was performed with a Perkin Elmer Lambda 950 UV/Vis/NIR spectrophotometer in reflectance mode over a wavelength range of 800–310 nm, with measurements every 2 nm. Because TiO_2 is known as an indirect band gap semiconductor, the optical band gaps of the materials were determined from the Tauc plot $(F(R)\cdot h\upsilon)^{1/2}$ vs. $h\upsilon$ expressed as energy in eV by extrapolation of the straight regions of the function and determined from the point of intersection after background subtraction.

Electrochemical impedance spectroscopy (EIS) was performed under the same conditions used for the photoelectrochemical measurements over a frequency range from 100 kHz to 10 mHz using a 5 mV amplitude sinusoidal signal without and with UV (365 nm) irradiation.

High-resolution transmission electron microscopy (HR-TEM), selected area electron diffraction (SAED), and energy dispersive X-ray analysis (EDX) were conducted with an FEI Talos F200S scanning/transmission electron microscope (S/TEM) operated at 200 kV. The TEM results were analyzed using ImageJ software. For d-spacings determination, the plot profile tool has been applied.

X-ray photoelectron spectroscopy (XPS) measurements were conducted using a JEOL JPS-9030 setup with a base pressure of 10^{-9} mbar, employing a monochromatic Al source with an angle of incidence of 10° with respect to the sample surface and a power of 120 W for excitation. A hemispherical analyzer with pass energies of 50 eV (surveys) and 30 eV (narrow scans) was used to detect the emitted photoelectrons at an angle of 10° relative to normal emission. The binding energy scale was calibrated by measuring sputter-cleaned gold and copper foils and setting the $Au4f_{7/2}$ peak to 84.0 eV and the $Cu2p_{3/2}$ peak to 932.6 eV. No signs of charging were observed during the measurements. All samples were exposed to air for approximately the same amount of time before introduction into the UHV system. The narrow scan spectra were fitted using CasaXPS.[43] A Gaussian-Lorentzian product was used for peak fitting, and the integrated areas after Shirley-background subtraction were used for quantification. Relative sensitivity factors were calculated by using the transmission function determined by measuring a sputter-cleaned Ag foil reference sample,[44] the atomic cross sections after Scofield provided by JEOL, and the inelastic mean free path for elements given by Seah and Dench and considering the asymmetry parameters. The calculated relative sensitivity factors (RSFs) were $RSF_{F1s} = 3.7$, $RSF_{O1s} = 2.7$, $RSF_{Ti2p} = 6.7$, $RSF_{N1s} = 1.8$, and $RSF_{C1s} = 1$.

Acknowledgements

E. W. would like to acknowledge the Polish National Agency For Academic Exchange, Polish Returns Programme (Project no. BPN/PPO/2021/1/00002), and the National Science Centre, Poland (Project no. 2022/01/1/ST5/00019) for financial support of the project. In addition, this research was supported by the Military University of Technology, grant number UGB 22-728. This support is gratefully acknowledged. The authors thank C. Erdmann for help with performing the transmission electron microscopy measurements and Dr Andrea Zehl for helping with EPR measurements.

Conflict of Interests

The authors declare no conflict of interest.

Data Availability Statement

The data that support the findings of this study are openly available in Zenodo at 10.5281/zenodo.10405094.

Keywords: renewable hydrogen · black titania nanotubes · $Ti^{3+\bullet}$ photoelectrocatalysis · light-induced defects

[1] X. Chen, L. Liu, P. Y. Yu, S. S. Mao, *Science* **2011**, *331*, 746–750.
[2] S. Mohajernia, P. Andryskova, G. Zoppellaro, S. Hejazi, S. Kment, R. Zboril, J. Schmidt, P. Schmuki, *J. Mater. Chem. A* **2020**, *8*, 1432–1442.
[3] E. Wierzbicka, M. Altomare, M. Wu, N. Liu, T. Yokosawa, D. Fehn, S. Qin, K. Meyer, T. Unruh, E. Spiecker, L. Palmisano, M. Bellardita, J. Will, P. Schmuki, *J. Mater. Chem. A* **2021**, *9*, 1168–1179.
[4] A. Sinhamahapatra, J.-P. Jeon, J.-S. Yu, *Energy Environ. Sci.* **2015**, *8*, 3539–3544.
[5] E. Wierzbicka, X. Zhou, N. Denisov, J. E. Yoo, D. Fehn, N. Liu, K. Meyer, P. Schmuki, *ChemSusChem* **2019**, *12*, 1900–1905.
[6] Z. Li, S. Wang, J. Wu, W. Zhou, *Renewable Sustainable Energy Rev.* **2022**, *156*, 111980.

[7] E. Wierzbicka, M. Domaschke, N. Denisov, D. Fehn, I. Hwang, M. Kaufmann, B. Kunstmann, J. Schmidt, K. Meyer, W. Peukert, P. Schmuki, *ACS Appl. Energ. Mater.* **2019**, *2*, 8399–8404.
[8] A. Mir, R. Ahmad, M. Aalim, A. Sohail, M. A. Shah, *Chem. Phys. Lett.* **2023**, *811*, 140219.
[9] H. Cui, W. Zhao, C. Yang, H. Yin, T. Lin, Y. Shan, Y. Xie, H. Gu, F. Huang, *J. Mater. Chem. A* **2014**, *2*, 8612–8616.
[10] D.-H. Yoon, M. R. U. D. Biswas, A. Sakthisabarimoorthi, *Opt. Mater.* **2022**, *133*, 113030.
[11] H. Tan, Z. Zhao, M. Niu, C. Mao, D. Cao, D. Cheng, P. Feng, Z. Sun, *Nanoscale* **2014**, *6*, 10216–10223.
[12] J. Will, E. Wierzbicka, M. Wu, K. Götz, T. Yokosawa, N. Liu, A. B. Tesler, M. Stiller, T. Unruh, M. Altomare, P. Schmuki, E. Spiecker, *J. Mater. Chem. A* **2021**, *9*, 24932–24942.
[13] S. Qin, N. Denisov, X. Zhou, L. Zdražil, D. Fehn, I. Hwang, M. Bruns, H. Kim, K. Meyer, P. Schmuki, *J. Phys. E* **2022**, *4*, 044004.
[14] G. Cha, I. Hwang, S. Hejazi, A. S. Dobrota, I. A. Pašti, B. Osuagwu, H. Kim, J. Will, T. Yokosawa, Z. Badura, Š. Kment, S. Mohajernia, A. Mazare, N. V. Skorodumova, E. Spiecker, P. Schmuki, *iScience* **2021**, *24*, 102938.
[15] S. Hejazi, S. Mohajernia, B. Osuagwu, G. Zoppellaro, P. Andryskova, O. Tomanec, S. Kment, R. Zbořil, P. Schmuki, *Adv. Mater.* **2020**, *32*, 1908505.
[16] S. Hejazi, H. Mehdi-pour, C. O. Otieno, J. Müller, S. Pour-Ali, M. Shahsanaei, S. Sarabadani Tafreshi, B. Butz, M. S. Killian, S. Mohajernia, *Int. J. Hydrogen Energy* **2023** *In Press* https://doi.org/https://doi.org/10.1016/j.ijhydene.2023.08.126.
[17] F. G. Echeverrigaray, A. R. Zanatta, F. Alvarez, *J. Mater. Res.* **2021**, *12*, 1623–1637.
[18] W. Zhou, W. Li, J. Q. Wang, Y. Qu, Y. Yang, Y. Xie, K. Zhang, L. Wang, H. Fu, D. Zhao, *J. Am. Chem. Soc.* **2014**, *136*, 9280–9283.
[19] S. S. Sahoo, S. Mansingh, P. Babu, K. Parida, *Nanoscale Adv.* **2021**, *3*, 5487–5524.
[20] E. Wierzbicka, B. Osuagwu, N. Denisov, D. Fehn, K. Meyer, P. Schmuki, *Iop. Conf. Ser. Mater. Sci. Eng.* **2020**, *908*, 012001.
[21] F. Fu, G. Cha, N. Denisov, Y. Chen, Y. Zhang, P. Schmuki, *ChemElectroChem* **2020**, *7*, 2792–2796.
[22] A. Naldoni, M. Altomare, G. Zoppellaro, N. Liu, Š. Kment, R. Zbořil, P. Schmuki, *ACS Catal.* **2019**, *9*, 345–364.
[23] D. Berends, D. H. Taffa, H. Meddeb, P. Schwager, K. Gehrke, M. Vehse, C. Agert, *Adv Photonics Res.* **2023**, *4*, 2300163.
[24] M. Sołtys-Mróz, K. Syrek, J. Pierzchała, E. Wiercigroch, K. Malek, G. D. Sulka, *Appl. Surf. Sci.* **2020**, *517*, 146195.
[25] P. Makuła, M. Pacia, W. Macyk, *J. Phys. Chem. Lett.* **2018**, *9*, 6814–6817.
[26] M. Altomare, N. T. Nguyen, S. Hejazi, P. Schmuki, *Adv. Funct. Mater.* **2018**, *28*, 1704259.
[27] E. Wierzbicka, T. Schultz, K. Syrek, G. D. Sulka, N. Koch, N. Pinna, *Mater. Horiz.* **2022**, *9*, 2797–2808.
[28] C. Ai, P. Xie, X. Zhang, X. Zheng, J. Li, A. Kafizas, S. Lin, *ACS Sustainable Chem. Eng.* **2019**, *7*, 5274–5282.
[29] X. Zhou, E. Wierzbicka, N. Liu, P. Schmuki, *Chem. Commun.* **2019**, *55*, 533–536.
[30] N. Liu, V. Häublein, X. Zhou, U. Venkatesan, M. Hartmann, M. Mačković, T. Nakajima, E. Spiecker, A. Osvet, L. Frey, P. Schmuki, *Nano Lett.* **2015**, *15*, 6815–6820.
[31] E. Szaniawska, K. Bienkowski, I. A. Rutkowska, P. J. Kulesza, R. Solarska, *Catal. Today* **2018**, *300*, 145–151.
[32] E. von Hauff, *J. Phys. Chem. C* **2019**, *123*, 11329–11346.
[33] S. Chen, A. M. Abdel-Mageed, D. Li, J. Bansmann, S. Cisneros, J. Biskupek, W. Huang, R. J. Behm, *Angew. Chem. Int. Ed.* **2019**, *58*, 10732–10736.
[34] M. Kehrer, J. Duchoslav, A. Hinterreiter, M. Cobet, A. Mehic, T. Stehrer, D. Stifter, *Plasma Processes Polym.* **2019**, *16*, 1800160.
[35] M. C. Biesinger, L. W. M. Lau, A. R. Gerson, R. St. C. Smart, *Appl. Surf. Sci.* **2010**, *257*, 887–898.
[36] J. C. Yu, J. Yu, W. Ho, Z. Jiang, L. Zhang, *Chem. Mater.* **2002**, *14*, 3808–3816.
[37] V. Etacheri, M. K. Seery, S. J. Hinder, S. C. Pillai, *Chem. Mater.* **2010**, *22*, 3843–3853.
[38] Y. K. Lai, J. Y. Huang, H. F. Zhang, V. P. Subramaniam, Y. X. Tang, D. G. Gong, L. Sundar, L. Sun, Z. Chen, C. J. Lin, *J. Hazard. Mater.* **2010**, *184*, 855–863.
[39] M. Pisarek, M. Krawczyk, M. Hołdyński, W. Lisowski, *ACS Omega* **2020**, *5*, 8647–8658.
[40] M. Wagstaffe, H. Hussain, M. J. Acres, R. Jones, K. L. Syres, A. G. Thomas, *J. Phys. Chem. C* **2017**, *121*, 21383–21389.
[41] A. A. Valeeva, E. A. Kozlova, A. S. Vokhmintsev, R. V. Kamalov, I. B. Dorosheva, A. A. Saraev, I. A. Weinstein, A. A. Rempel, *Sci. Rep.* **2018**, *8*, 9607.
[42] N. Díez, A. Śliwak, S. Gryglewicz, B. Grzyb, G. Gryglewicz, *RSC Adv.* **2015**, *5*, 81831–81837.
[43] N. Fairley, V. Fernandez, M. Richard-Plouet, C. Guillot-Deudon, J. Walton, E. Smith, D. Flahaut, M. Greiner, M. Biesinger, S. Tougaard, D. Morgan, J. Baltrusaitis, *Appl. Surf. Sci. Adv.* **2021**, *5*, 100112.
[44] P. J. Cumpson, M. P. Seah, S. J. Spencer, *Spectrosc. Eur.* **1998**, *10*, 8–15.

Manuscript received: November 7, 2023
Revised manuscript received: December 22, 2023
Version of record online: January 31, 2024